Nondestructive Evaluation of Grout Defects in Internal Tendons of Post-Tensioned Girders

Tevfik Terzioglu[1], Madhu M. Karthik[2], Stefan Hurlebaus[3], Mary Beth D. Hueste[3], Virginia Foster[4], Stefan Maack[5], Jens Wostmann[5], Herbert Wiggenhauser[5], Martin Krause[5], Patrick K. Miller[6], Larry D. Olson[6]

Abstract

Post-tensioning systems provide safe and efficient construction solutions for long span bridges. Despite the improved grouting practices over the past decade, existing post-tensioning systems may have a significant amount of grout defects, which could lead to corrosion of the strands. Condition assessment of post-tensioning systems is necessary to allow bridge owners to take timely, proactive actions to mitigate or prevent further deterioration and unanticipated tendon failures. This paper presents a detailed experimental study conducted to assess the performance of nondestructive evaluation techniques in detecting grout defects within internal tendons. Several nondestructive evaluation techniques that include Ground Penetrating Radar, Impact Echo, Ultrasonic Tomography, and Ultrasonic Echo are evaluated in terms of detecting the location and severity of fabricated grout defects in a full-scale post-tensioned U-girder mock-up specimen. Ground Penetrating Radar is able to identify the location and the profile of the internal tendons, particularly the metal ducts due to strong reflections, but did not provide any information about the defect conditions within the tendon. Both Impact Echo and Ultrasonic Echo techniques are

---

[1] Postdoctoral Research Associate, Texas A&M Transportation Institute, College Station, TX 77843 (corresponding author). E-mail: tevfikterzioglu@tamu.edu
[2] Assistant Professor, Dept. of Civil Engineering, Indian Institute of Technology, Palakkad, India 678557.
[3] Professor, Zachry Dept. of Civil Engineering, Texas A&M Univ., College Station, TX 77843.
[4] Structural Engineer, Aguirre & Fields, LP, Fort Worth, TX 76244
[5] Researcher, Bundesanstalt für Materialforschung und –prüfung (BAM), Berlin, Germany
[6] Principal Engineer, Olson Engineering, Wheat Ridge, CO 80033

effective in terms of identifying the location of grout defects, but could not differentiate between water, void, or compromised grout conditions.

Keywords: Nondestructive Testing, Ground Penetrating Radar, Impact Echo, Ultrasonic Tomography, Ultrasonic Echo, Bridge Inspection

1. Introduction

Post-tensioned (PT) structural elements can be used to economically achieve long spans, and at the same time provide an aesthetically pleasing structure. Post-tensioning systems are desirable in bridge construction as they significantly increase the structural capacity, and are relatively simple to implement. Based on the location of the tendons, post-tensioning systems are classified as internal or external post-tensioning systems. A tendon that is embedded inside the concrete is defined as an internal tendon, whereas a tendon that is placed outside the concrete is defined as an external tendon. Internal tendons that are completely filled with grout and have no voids are considered bonded tendons.

The presence of voids in the tendons can cause discontinuity in the transfer of stress to the adjacent concrete along the length of the tendon. Voided regions in tendons can be detrimental to the strength of the tendon system in two major ways. First, voids can lead to loss of tendon strength due to ineffective redistribution of stress within the beam [1]. Second, and most importantly, corrosion can occur when strands are embedded in cementitious material and when these strands are exposed to atmospheric conditions through the voids. Although the concrete cover around the tendon provides an extra layer of protection for internal tendons, they are still vulnerable to corrosion due to the presence of water, compromised grout, and air voids. Severe deterioration and tendon failures have occurred in the past due to problems related to poor grouting practices that create air voids within the duct.

The collapse of the Bickton Meadows Footbridge in 1967 was the first significant case of corrosion-related failure of bonded PT bridges [2]. The bridge collapsed within 15 years of its construction. The precast segments in this bridge were jointed with mortar. These mortar joints were thin and highly permeable, which allowed moisture, chlorides, and oxygen to penetrate the mortar and reach the steel tendons that traversed the joints. This resulted in accelerated corrosion of the steel tendons.

The top and bottom anchorage zones of the vertical tendons in the Bob Graham Sunshine Skyway Bridge piers experienced severe corrosion damage within eight years after construction. The major direct and indirect causes for the tendon failure were poor grout quality and grouting practices and presence of voids formed due to bleed water evaporation inside the PT tendon [3].

Grouting is a main component that protects the strands against corrosion. However if not done properly, grouting itself can be a reason for accelerated corrosion. There are locations where voids are more likely to occur, such as at high points of parabolic drapes, where sharper curves exist. Cavitation of the grout during the grouting process can cause subsequent subsidence of the grout. This can lead to large pockets of air entrapped in the grout [4]. These practices can result in large voids within the duct, potentially making the strands more susceptible to corrosion damage.

2. Background

Internal post-tensioning systems are embedded in concrete, making it difficult to inspect using NDE methods. In addition, the steel reinforcement that surrounds the internal tendons creates additional difficulty by increasing the noise level in the inspection data. Various promising NDE techniques that have been used in the past for the inspection of internal tendons include Ground Penetrating Radar (GPR), Impact Echo (IE), Ultrasonic Echo (USE), and Ultrasonic Tomography (UST).

GPR is a radar imaging technique that involves emitting electromagnetic pulses (typically in the order of 1.0 GHz) from an antenna and receiving the reflected pulses from internal reflectors. Reflections are caused by changes in the material's electrical conductivity and dielectric permittivity. GPR is extremely sensitive to metallic materials in structural applications and is one of the most successful high-speed techniques in damage detection of concrete structures [5, 6]. In bridge structures, GPR has been used to identify locations of reinforcement within concrete and cavities in bridge decks [7]. However, the radar impulse is highly reflected by metallic materials, making the application of GPR unsuitable for the identification of voids in internal metal ducts [8, 9], but successful for non-conducting (plastic) ducts [10].

GPR has been shown to easily identify the location and depth of reinforcement and internal tendons (both plastic and metal) embedded in concrete decks or walls, although mats of reinforcement that are below other reinforcement mats are difficult to detect [11]. Field tests reveal that it is helpful to apply other NDE methods in collaboration with GPR [8, 12, 13]. Derobert et al. [14] and Wimsatt et al. [15] recommend using either air-coupled or ground-coupled GPR as a primary NDE method to quickly obtain general information of a structure, such as layout and depth of reinforcement and tendons, then following up with appropriate in-depth testing methods for a detailed evaluation.

In the IE inspection method, a stress pulse is generated in the concrete element by a mechanical impact. The reflected wave is then identified using an accelerometer receiver mounted close to the impact point on the surface of concrete. The impact generates a high energy pulse that can penetrate into concrete, therefore the IE method is particularly promising for identifying defects in concrete structures [16-23]. Carino and Sansalone [17] applied the IE method to detect voids in grouted PT tendons located in a 1 m thick concrete wall specimen. Tinkey et al. [24]

developed a movable IE scanner system to be able to test large specimens in a timely manner. The authors concluded that the scanning system could not detect voids well when the diameter of the tendons was small and the concrete cover was large. Harris [25] reported that IE could detect large voids in grouted tendons with 60 percent accuracy provided the system was used simultaneously with GPR and covermeter systems to provide depth and lateral alignment measurements. However, the size of the voids could not be determined. In another study, an air-coupled IE system using a microphone was developed to assess an internal tendon system [26]. The system evaluated voids in metallic ducts but failed to identify voids in plastic ducts. Voided internal tendons have a high frequency range, but peaks indicating defects may not be clearly identified because of the many peak frequencies that exist due to reflection [27, 28].

The ultrasonic technique encompasses all methods that employ the use of acoustic waves over 20 kHz. The principle of operation is the same regardless of the type of ultrasonic system: a sensor or group of sensors emits a stress pulse (typically a P-wave, S-wave, or R-wave) into the specimen. As the waves propagate, portions of the wave are reflected from regions where a variation in impedance occurs, and these reflections are captured using sensors. Through time-of-flight measurements and frequency/amplitude characteristics, defects and/or discontinuities can be determined. The ultrasonic technique has shown a promising future for estimating concrete thickness, internal duct locations, material layers, presence of reinforcement, and elastic modulus. This technique can also be used for detecting and locating internal defects in concrete structures, such as cracks, voids, delamination, and reinforcement corrosion [15, 29-35].

There are three main modes of operation of the UST technique: pulse-echo, through-transmission, and linear array. In the pulse-echo technique, ultrasonic measurements are made with a single sensor or group of sensors that act as both the transmitter and the receiver. In the through-transmission technique, ultrasonic waves are emitted by a sensor or group of sensors, and the reflected pulses are received by a separate sensor or group of sensors located on the opposite face of the test object. A linear array operates in a mode referred to as the pitch-catch mode. Here, a group of sensors are arranged in a linear fashion, but unlike the pulse-echo mode, a sensor or a group of sensors emits a unified stress pulse and the other sensor or groups of sensors receive the reflected pulse. Krause et al. [30] compared multiple pulse-echo, through-transmission, and linear array techniques on 84 mm diameter internal PT tendons and reported that all of the tested techniques could detect the metal tendon location and thickness of the member accurately. The only mode capable of detecting the voided areas was the linear array aided by a reconstruction analysis called the Linear Synthetic Aperture Focusing Technique (LSAFT). Mayer et al. [36] developed phase evaluation algorithms that used ultrasonic data to examine the return phase shift. The resulting phase diagram showed the local change in phase of ultrasonic waves reflected from interfaces within the material. In laboratory conditions, Krause et al. [37] used this technique to effectively distinguish between the reflections from steel objects and air interfaces within concrete.

3. Placement of Grout Defects in Internal Tendons

In order to simulate a realistic geometry, reinforcement details, and accessibility conditions, a full-scale 22.9 m long, 4.2 m wide, and 1.85 m deep post-tensioned U-girder specimen was constructed. To evaluate the effectiveness of the various NDE techniques in detecting grout defects in the internal tendons, several parameters such as tendon diameter, concrete cover, tendon profiles, duct material (corrugated metal or non-metal), reinforcement surrounding the tendon, and layered tendons were incorporated into the specimen. Fig. 1 shows the general layout of the tendons and the tendon designation. Corrugated plastic ducts were used for Tendons 1 and 2 (internal diameter (ID) = 76 mm, outer diameter (OD) = 91 mm, thickness (T) = 2.5 mm) in the flange of the South

Wall, and for Tendons 3, 4, and 5 (ID = 99 mm, OD = 114 mm, T = 2.5 mm) in the web of the South Wall. Corrugated metal ducts were used for Tendons 13 and 14 (ID = 79 mm, OD = 84 mm, T = 0.5 mm) in the flange of the North Wall, and for Tendons 10, 11, and 12 (ID = 102 mm, OD = 107 mm, T = 0.5 mm) in the web of the North Wall. Fig. 2 shows several construction steps including the profile of the draped internal tendons.

To evaluate the capabilities and limitations of several NDE techniques in detecting grout defects in the internal tendons, various grout defects were placed in about ninety locations along the length of the internal tendons located in the webs and top flanges of the full-scale PT girder specimen. Table 1 lists the descriptions and definitions of the grout defects placed in the internal tendons. Each duct was divided into 914 mm long sealed sections to facilitate placement of the grout defects. Three common grout conditions; namely voids, water infiltration, and compromised grout having various degrees of severity; were carefully fabricated at predetermined locations in the internal tendons. Voided sections were created by filling the insulated segments of the internal tendons with 25, 50, or 75% by volume normal grout (following the grout manufacturer's specifications). To implement water infiltration defects, partially grouted sections were filled with water.

Normal grout used for the partially and completely filled sections was obtained by combining *MasterFlow 1205* grout with two gallons of water per bag of grout, which was within the range suggested by the manufacturer. The compromised grout conditions included unhydrated grout, segregated grout, and gassed grout. Unhydrated grout was obtained by reducing the volume of water by 30%, and segregated grout was made by using 36% more water by volume than normal grout. Gassed grout condition was also implemented as one of the compromised grout defects to simulate a condition that is typically observed in older bridges. Gas releasing agents such as aluminum powder in the grout mix react with alkalis in the cement to produce hydrogen gas bubbles, which in turn cause expansion of the grout prior to hardening. While this property of the grout improves the workability and flowability of the grout, hydrogen molecules can be released leading to hydrogen embrittlement and fracture of the steel strands. Most of the current guidelines and regulations prohibit the use of gas releasing agents used for grouting of post-tensioning tendons, however they were widely used in the past. *MasterFlow 100* grout with 1.06 gallons of water per bag of grout was used to obtain gassed grout. Gassed grout is achieved due to the inherent composition of the grout mix itself. Various levels of severity of compromised grout conditions were created by varying the volume of the compromised grout in the isolated sections. For example, to achieve segregated grout condition GU1, which comprises approximately 50% by volume of unhydrated grout, the section of the duct was first filled to about 50% with normal grout. Following the curing of normal grout the remaining half of the duct was filled with unhydrated grout, to obtain a section that consisted of 50% unhydrated grout.

4. NDE Techniques used for Identifying Grout Defects in Internal Tendons

All internal tendons of the post-tensioned U-girder specimen were inspected using GPR, IE, USE, and UST techniques. A description of each device and its performance in terms of identifying the location and severity of the grout defects is discussed in what follows.

4.1 Ground Penetrating Radar

The GPR inspection technique was used to inspect grout defects in the internal tendons in the walls, flanges, and anchorage regions of the PT girder specimen. Geophysical Survey Systems, Inc. (GSSI) StructureScan Mini HR high-resolution GPR system with a 2.6 GHz antenna, which has a scan depth of 400 mm, was chosen for this application. Fig. 3(a) shows the StructureScan

Mini HR GPR unit mounted on wheels. The device records data as the unit is rolled along the inspection surface. A 50 mm × 50 mm grid system was created on the webs, flanges, and anchorage regions of the PT girder specimen. GPR scans were made along the grid system in both the x-direction (along the length of the specimen) and y-direction (transverse to the length of the specimen) to generate a 3D model of the inspected specimen.

Fig. 4 and Fig. 5 present the GPR scan results of the North and South wall, respectively. The web and flange on the exterior surface of the PT girder specimen were scanned separately owing to their differences in geometry. In Fig. 4(c) and Fig. 5(c), the processed GPR images of the web and the flange are combined. The regions at the interface between the web and the flange are shown in gray due to insufficient data at these locations. Similarly, the white regions in Fig. 4(d) and Fig. 5(d) are the locations that could not be accessed for inspection from the interior of the girder due to the deviators. Fig. 4(c) and (d) present the external and internal GPR scan results of the North Wall. Because the metal ducts produce strong reflections, the profile of these ducts are identifiable in the GRP scans. However, the scans do not provide any information regarding the grout defects within these metal ducts. Fig. 5(c) and (d) present the external and internal GPR scan results of the South Wall. The profile of the plastic ducts in the South Wall are not as clear as the metal ducts in the North Wall, particularly in the interior wall scan. This is owing to the weak reflections from the plastic ducts compared to the metal ducts. As in the case of the North Wall, the scans of the South Wall did not provide any information regarding the grout defects in the plastic ducts.

4.2 Impact Echo

The Impact Echo tests were performed using an IE scanner test head that was connected to a data acquisition (DAQ) system. Fig. 3(b) shows the photo of the impact echo scanner mounted on wheels and the DAQ system. The IE scanner produces an impact at 25 mm intervals as it is rolled along the concrete surface. To assess the grout defects within internal tendons of the PT girder specimen, scans were performed along vertical lines at 152 mm spacing along the entire length of the webs of the North and South Wall. In addition, GPR scans were performed vertically on both the webs at 762 mm nominal spacing to determine the locations of internal PT tendons.

IE scan results present PT tendons with an increase in measured thickness, which corresponds to a decrease in resonant frequency. Typically, even well grouted tendons cause a shift in the measured thickness, although this shift is less than 20%. However, a partially grouted or empty duct will result in a greater shift in the measured thickness. The shift in measured thickness between a completely grouted duct and a voided duct is dependent on a number of factors including the thickness of concrete, the duct diameter, the duct material (metal or plastic), and the velocity of the pulse wave in grout in relation to concrete. Therefore, the thresholds for determining if a duct is partially grouted, empty, or sound are project specific. This can be established from IE scans on a variety of conditions, and corroborating this with destructive evaluation such as drilling, borescope investigation, or a combination of both.

For the current investigation, the IE scans were executed in the girder web section with constant thickness and the tapered sections, albeit with normalization. The method could not be used to scan the anchorage regions of the girder, where the concrete thickness was greater than about 1.5 m. Fig. 6 and Fig. 7 present the IE scan results of the North and South wall, respectively. As the subject of this investigation is to identify grout defects within the internal tendons, a GPR unit was first used to locate the approximate location of the internal tendons. The black lines in Fig. 6 and Fig. 7 represent the location of the internal tendons. In both figures, figure (a) identifies the location of the actual defects with red labels, figure (b) shows the color condition image obtained from the IE scans, and figure (c) summarizes results obtained from the IE scans. The IE scan results are presented on a graduated color scale, where the color represents the thickness. The results presented in Fig. 6 and Fig. 7 indicate changes in apparent thickness at some duct locations, indicating variances in grout conditions. It should be noted that slightly different color scales are used for the webs of the North and South Walls, as the North Wall web showed smaller changes in thickness compared to the South Wall. This may be attributed to the difference in the duct material within the two webs.

In Fig. 6(b) and Fig. 7(b), the color scale is set such that purple indicates the normal web thickness, blue to green indicate a shift in thickness that indicates completely filled tendon with sound grout, yellow to orange likely indicates partial grout, while orange to red indicates the poorest grout condition. Although the grout defects can be identified from the color condition images, Fig. 6(c) and Fig. 7(c) present the results from an in-depth investigation of the IE scan results. The summary of the scan results are indicated in four colors, where red represents full voids, yellow represents partial voids, white represents intact sections, and purple implies that the tendons are not detected.

IE was found to be a relatively effective NDE method for identifying the location of grout defects in internal tendons. However, it did not prove to be a highly reliable technique for inspection of internal tendons as the overall accuracy of the IE method was not promising. IE could only identify the location of about 50 percent of the water infiltration defects in both the plastic and metal ducts. In addition, only one-third of the voids could be located successfully. The IE method could identify the severity of the grout defects with an average error of 33 percent; which, although not very reliable, gives an idea of the size of the internal defects [38, 39].

4.3 Ultrasonic Echo

In the ultrasonic echo method the structural element under investigation is mechanically excited by a pulse in the inaudible ultrasonic range, and the reflected portions of the pulse are recorded. Reflections occur at interfaces of concrete with metal (e.g., reinforcement, tendon duct) and with air (e.g., back-wall, air-filled void). In contrast to radar, no total reflection occurs at interfaces with reinforcement; therefore, USE may be used to study components with high reinforcement density.

A single measurement using the USE method cannot be used to draw conclusions about the position and condition of tendons. Therefore, it is essential that USE measurements be recorded along a measurement grid with a constant measuring point distance. This would allow for the reconstruction of the scanned surface, with a subsequent imaging of individual reinforcement bars or tendons. However, compared to radar, the resolution of USE scans are often coarse due to the diffusion of signals by the aggregates in concrete.

The ultrasonic echo device used in this investigation consists of a control unit and a probe. The control unit generates an electronic pulse of several hundred volts. This impulse is led to the probe through a coaxial cable. The probes are excited using the piezoelectric pulse principle. The probe is made up of 24 dry point transducers that are mounted on a spring mechanism, and does not require any coupling agents. The spring mechanism ensures contact even on rough concrete surfaces. A total of 12 transducers act as transmitters, whereas the remaining 12 transducers serve as receivers.

Overlapping measurements help ensure better resolution of the scan results. Therefore, automated systems can be used as they can record data in a very fine measuring grid with high precision. Fig. 3(d) depicts the automated scanner system used in the current investigation. The frame of the automated scanner was fixed on the vertical walls by employing a suction system.

The frame moves a probe made of dry point contact transducers over the inspection surface. Using a pneumatic system, the sensor is moved from one measuring point to the next measuring point (typical measuring grid: 20 × 20 mm). A single setup of the automated scanner system measured about one square meter of the bridge surface. Several of these measuring fields were combined to obtain the scan image of the inspection surface.

There are some areas of the specimen where the data could not be analyzed properly due to rough surface conditions resulting in bad coupling of the transducers. Reflections occur at interfaces of concrete with metal (e.g., reinforcement, tendon duct) and with air (e.g., back-wall, air-filled void), which have a lower impedance than concrete. For the internal tendons there is a possibility of thin air layers around the ducts, in such cases the reflected ultrasonic signal may not describe the inner state of the tendons.

Fig. 8 and Fig. 9 present the results from USE inspection of the North Wall and South Wall, respectively, and a comparison of the scan results with the actual defect conditions. While Fig. 8(b) and Fig. 9(b) represent the overview of the phase analysis results, thereby simplifying the comparison of the scan results with the defect key, figures (c) and (d) presents the amplitude and phase diagrams in false color representations. The spatial resolution of the result is about 200 mm, implying that deviations of the phase value smaller than 200 mm may not be indicated in the results. The results are classified and indicated in three colors: (a) red corresponds to high impedance, about a 180 degree phase shift, which implies an intact tendon; (b) blue corresponds to low impedance, about a 0 degree phase shift, which implies air voids and/or water; (c) gray indicates an unclear result; and (d) white represents no or very weak phase indications. For air voids and/or water, the acoustic impedance is low, which means total reflection. However, thin air layers at the grout duct interface may also result in total reflection.

Although the USE technique was more effective than the IE method in terms of identifying the location of grout defects, it still did not provide conclusive results that could be used for inspection of internal tendons. The USE method could successfully identify the location of two-thirds of the water infiltration defects and one-third of the voids and compromised grout in internal tendons. This technique does not give any information about the severity of the grout defects. In addition, the location of intact sections could not be detected conclusively [38, 39].

4.4 Ultrasonic Tomography

An ultrasonic tomograph A1040 MIRA system was utilized to identify grout defects in the internal tendons embedded in the webs, flanges, and anchorage regions of the PT girder specimen. Fig. 3(c) shows the MIRA device used for scanning the specimen, which is capable of testing concrete thicknesses up to two meters. The measuring device consists of a 4 × 12 array of dry contact low frequency transducers that transmit transverse waves with a nominal operating frequency of 50 kHz. When the device is triggered, a column of four transducers act as the transmitter, whereas the remaining columns of transducers act as receivers. The device creates a data array using the information measured from the transducers. The built-in processor allows onsite data analysis and displays an image on the built-in screen. A special purpose software can be used to create a 3D image of the scanned structure.

The girder was tested along the length and height of the web walls using a 50 mm square grid system. The specimen was scanned with the device oriented both parallel and perpendicular to the longitudinal axis of the internal tendons. Owing to the large area being tested, the walls of the girder specimen were scanned as six separate sections to effectively manage the data collection and data processing.

Fig. 10 presents the results from UST scanning of the North Wall of the PT girder specimen. The depths of the scans are also detailed in the caption. The regions that were not accessible during inspection are shown in black. As seen in Fig. 10(c), the device was able to vaguely identify the profile of the metal ducts, particularly when the device was oriented perpendicular to the longitudinal axis of the ducts. However, the A1040 MIRA was unable to identify grout defects within the internal tendons. Higher reflections were observed between markers S (16.5 m) and V (19.2 m), suggesting that UST could possibly identify water defects; however, no conclusive evidence could be obtained from the scan results.

Fig. 11 presents the UST scan results of the South Wall of the PT girder specimen. As evident in Fig. 11(d), UST was able to identify the internal plastic ducts, particularly when the device was oriented perpendicular to the ducts. However, the grout defects within the internal tendons could not be identified.

5. Discussion

This study presents an evaluation of four nondestructive testing methods that include GPR, IE, USE and UST in terms of their performance for locating grout defects in internal tendons. GPR and UST methods were able to identify the tendon profiles in the web walls of the girder but ineffective for locating any defects in the tendons buried in the walls. On the other hand, IE and USE methods provided somewhat successful results for identifying grout defect in the tendons. In most cases, it is more effective to use a combination of techniques to achieve accuracy and practicality at the same time. The GPR method is the fastest and least labor-intensive method for locating the tendons. Once the tendon profile is located, IE or USE methods can be used to scan the tendon regions for locating any possible grout defects inside the tendons.

Table 2 presents a comparison of the defect key with the results obtained from the inspection of the web walls of the girder specimen using IE and USE techniques. Tabulated data shows the comparative results of each defect zone for all six internal tendons in a binary pass/fail format, as follows:

True positive (TP): Method correctly indicates that a defect exists.

True negative (TN): Method correctly indicates that a defect does not exist.

False positive (FP): Method indicates that a defect exists, when it actually does not.

False negative (FN): Method indicates that a defect does not exist, when it actually does.

One clear shortcoming of both the IE and USE methods is that they are ineffective for detecting grout defects in the anchorage regions (A-C and X-Z), and for tendons that are close to the top and bottom edges of the web wall. This poor detection rating can be attributed to the comparatively thicker concrete layer that exists behind Tendon 3 and Tendon 10, with a thick concrete top flange and bottom slab, respectively.

Table 3 summarizes several uncertainty parameters such as sensitivity, false alarm, specificity and precision for different defect types when tested with IE, USE and combination of the two techniques. *Sensitivity* is a measure of how well a method identifies a defect and is calculated as the ratio of TPs to the total number of defects (TP+FN). *False alarm* is the ratio of FPs to the total number of intact regions (FP+TN). *Specificity* is a measure of how well a method identifies the intact regions and is the ratio of TNs to the total number of intact regions (TN+FP). *Precision* is the probability that a defect being identified is actually a defect and is given as the ratio of TPs to the sum of TPs and FPs. This type of quantitative evaluation allows for an objective comparison including false alarm ratings of the method being used.

It can be observed from Table 3 that a combination of IE and USE techniques has a sensitivity of about 70% in detecting water infiltration defects. However, the sensitivity of IE, USE, and a combination of IE and USE for detecting voids and compromised grout ranges from 12% to 36%. The probability of false alarm of both inspection techniques and their combination is 50% to 83%, with the USE technique showing the highest false alarm rate of about 83%. The specificity of the USE technique is a very low at 17%; and for all the methods and their combination it is at or below 50%. However, precision, which is a measure of the correctness of the techniques in identifying defects, is below 40%.

6. Conclusions

Ground Penetrating Radar (GPR), Impact Echo (IE), Ultrasonic Echo (USE), and Ultrasonic Tomography (UST) techniques were used to inspect grout defects in a full-scale post-tensioned U-girder specimen. The objective was to assess the capabilities of these techniques for identifying the location and severity of grout defects within the internal tendons embedded in concrete. The following conclusions were derived from this study.

1. Among the four NDE methods tested, the USE technique provided the best results in terms of identifying the location of the largest number of grout defects. However, none of the NDE techniques that were evaluated in this investigation were effective in identifying the severity of the grout defects.
2. The GPR technique is highly repeatable and reproducible, and was able to identify the location and the profile of the internal tendons, particularly the metal ducts due to strong reflections. However, this method did not provide any information about the grout defects within the internal tendons.

3. The IE technique was successful in terms of identifying the location of water infiltration defects in the internal tendons embedded in the concrete web sections. The success rate was lower for the void and compromised grout defects. Although the IE technique could detect about half of the grout defects, it could not differentiate between the various internal grout defects. In addition, the IE testing was not effective in imaging the PT tendons within the thick anchorage regions.
4. The UST technique using MIRA A1040 was unable to identify the grout defects within the internal tendons. The resolution of the UST image in locating the internal tendons was better when the device was oriented perpendicular to the longitudinal axis of the tendons. The equipment was more effective in identifying the internal plastic ducts than the metal ducts.
5. Although both the UST and USE devices use similar technologies, the USE device was more effective than the MIRA device owing to the phase evaluation algorithms that use the collected ultrasonic data to examine the return phase shift. The results form USE testing suggest that this method is capable of identifying grout defects in internal tendons for both plastic and metal ducts. The USE method provided a good performance for identifying the location of water infiltration defects. Although estimations are provided at several locations for plastic ducts, at present there is insufficient experience for evaluating the details of the phase behavior in plastic ducts.
6. None of the existing NDE methods that were used in this investigation for the evaluation of the grout defects in internal tendons could conclusively identify the known grout defects with a high degree of confidence. Further improvement is warranted in the evaluation techniques, data processing techniques, or a combination of both, to improve the reliability of NDE for identifying defects in the internal tendons of PT girders.

Although IE and USE methods show some promise, there is a need for further research and development to improve their performance when used to inspect internal tendons embedded in reinforced concrete regions.

Acknowledgements

This project was sponsored by the American Association of State Highway and Transportation Officials, in cooperation with the Federal Highway Administration, and was conducted through The National Cooperative Highway Research Program (Grant No. NCHRP 14-28). The project team would like to thank the senior program officer, Dr. Waseem Dekelbab, and all NCHRP panel members for their input during the various phases of the project. The authors would like to thank Mr. William R. 'Randy' Cox (ASBI) for his support of grouting certification training; and Mr. John Turner and Dr. Mike Mota (CRSI), Mr. Pete Diggs and Mr. Bryan McMurray (Gerdau Long Steel North America), Dr. Zuming Xia and Mr. John Crigler (VSL), Mr. Ray Bauer (Commercial Metals Company), Mr. Mark Huff (BASF), and Mr. Steve Koch (Sumiden Wire Products) for their in-kind contribution of material for the construction of the mock-up specimen.

Table 1–Description of Grout Defects

Internal Defect Condition		**Label**	**Description**[1,2]
Water Infiltration		W1	~ 25% full of water
		W2	~ 75% full of water
		W3	100% full of water
Compromised Grout	Segregated Grout	GS1	~ 50% segregated grout
		GS2	100% segregated grout
	Unhydrated Grout	GU1	~ 50% unhydrated grout
		GU2	100% unhydrated grout
	Gassed Grout	GG	100% gassed grout
Voids		V1	~ 25% void
		V2	~ 50% void
		V3	~ 75% void
		V4	100% void

Notes:
1. Percentages are by volume.
2. Actual values are as close as possible to the target value provided.

Table 2–Results of IE and USE Testing for Identifying the Location of Grout Defects in Internal Tendons

Defect Zone	**Tendon 3**				**Tendon 4**				**Tendon 5**				**Tendon 10**				**Tendon 11**				**Tendon 12**			
	Defect Type	**IE**	**USE**	**IE + USE**	**Defect Type**	**IE**	**USE**	**IE + USE**	**Defect Type**	**IE**	**USE**	**IE + USE**	**Defect Type**	**IE**	**USE**	**IE + USE**	**Defect Type**	**IE**	**USE**	**IE + USE**	**Defect Type**	**IE**	**USE**	**IE + USE**
A - B	INT	FP	×	FP	V4	FN	FN	FN	V1	FN	FN	FN	INT	FP	TN	TN	V4	FN	FN	FN	V4	FN	FN	FN
B - C	INT	FP	×	FP	INT	FP	×	FP	INT	FP	×	FP	INT	FP	FP	FP	W1	FN	FN	FN	INT	FP	FP	FP
C - D	INT	TN	×	TN	INT	TN	×	TN	INT	TN	×	TN	INT	FP	FP	FP	GU2	FN	FN	FN	INT	TN	FP	TN
D - E	V1	TP	TP	TP	V1	FN	FN	FN	INT	TN	×	TN	INT	FP	FP	FP	V1	FN	FN	FN	V3	TP	TP	TP
E - F	V1	FN	FN	FN	GS1	FN	TP	TP	V2	FN	FN	FN	INT	FP	FP	FP	INT	TN	FP	TN	V2	FN	FN	FN
F - G	V1	FN	FN	FN	GG	FN	TP	TP	V3	FN	FN	FN	INT	FP	FP	FP	GS1	FN	TP	TP	V1	FN	TP	TP
G - H	V4	FN	FN	FN	INT	FP	×	FP	W2	TP	FN	TP	INT	FP	FP	FP	INT	TN	FP	TN	INT	TN	TN	TN
H - I	INT	×	×	×	INT	FP	×	FP	INT	TN	×	TN	INT	FP	FP	FP	GG	FN	FN	FN	W2	TP	FN	TP
I - J	INT	×	×	×	GS2	TP	TP	TP	V1	FN	FN	FN	INT	FP	FP	FP	GS2	FN	FN	FN	GS1	FN	FN	FN
J - K	GU1	×	FN	FN	INT	FP	×	FP	INT	TN	×	TN	INT	FP	FP	FP	INT	TN	FP	TN	GU1	FN	FN	FN
K - L	INT	×	×	×	W3	TP	TP	TP	GU1	FN	FN	FN	INT	FP	FP	FP	INT	TN	TN	TN	GU2	FN	FN	FN
L - M	V1	×	FN	FN	INT	TN	×	TN	GU2	FN	FN	FN	INT	FP	FP	FP	INT	TN	TN	TN	GS1	FN	FN	FN
M - N	INT	×	×	×	INT	FP	×	FP	GS1	FN	FN	FN	INT	FP	FP	FP	INT	TN	TN	TN	INT	FP	FP	FP
N - O	INT	×	×	×	INT	FP	×	FP	INT	TN	×	TN	INT	FP	FP	FP	V1	FN	FN	FN	INT	TN	FP	TN
O - P	INT	×	×	×	INT	FP	×	FP	GS1	FN	FN	FN	INT	FP	FP	FP	V4	TP	TP	TP	INT	TN	FP	TN
P - Q	W2	×	FN	FN	GU2	TP	TP	TP	INT	TN	×	TN	INT	FP	FP	FP	GU2	FN	FN	FN	INT	TN	FP	TN
Q - R	INT	×	×	×	INT	FP	×	FP	INT	TN	×	TN	INT	FP	FP	FP	GU1	FN	TP	TP	INT	TN	FP	TN
R - S	INT	×	×	×	INT	TN	×	TN	INT	TN	×	TN	INT	FP	FP	FP	INT	TN	FP	TN	INT	TN	FP	TN
S - T	V2	FN	FN	FN	W3	FN	TP	TP	W1	FN	FN	FN	INT	FP	FP	FP	W3	TP	TP	TP	W1	FN	TP	TP
T - U	INT	TN	×	TN	INT	TN	×	TN	INT	TN	×	TN	INT	FP	TN	TN	W2	TP	TP	TP	INT	TN	FP	TN
U - V	INT	FP	×	FP	V3	FN	TP	TP	GU1	FN	FN	FN	INT	FP	FP	FP	W2	FN	TP	TP	GU1	FN	FN	FN
V - W	INT	FP	×	FP	INT	TN	×	TN	GG	FN	FN	FN	INT	FP	FP	FP	INT	TN	FP	TN	GG	FN	FN	FN
W - X	INT	TN	×	TN	W2	FN	TP	TP	GS2	FN	FN	FN	INT	FP	TN	TN	W2	FN	FN	FN	W3	TP	TP	TP
X - Y	INT	FP	×	FP	V3	FN	TP	TP	V4	FN	FN	FN	V2	FN	FN	FN	V3	FN	FN	FN	V4	FN	FN	FN
Y - Z	GS2	FN	FN	FN	W1	FN	TP	TP	GS2	FN	FN	FN	GS2	FN	FN	FN	W3	FN	FN	FN	V2	FN	FN	FN

Note: TP = True Positive, TN = True Negative, FP = False Positive, FN = False Negative, × = Inconclusive.

Table 3–Quantitative Uncertainty Evaluation of IE and USE Methods for Different Grout Defects

Uncertainty Parameter	Void			Water Infiltration			Compromised Grout		
	IE	**USE**	**IE+USE**	**IE**	**USE**	**IE+USE**	**IE**	**USE**	**IE+USE**
Sensitivity	0.12	0.22	0.22	0.40	0.56	0.69	0.17	0.33	0.36
False Alarm	0.54	0.83	0.50	0.54	0.83	0.50	0.54	0.83	0.50
Specificity	0.46	0.17	0.50	0.46	0.17	0.50	0.46	0.17	0.50
Precision	0.07	0.15	0.14	0.13	0.21	0.23	0.20	0.37	0.38

Note: *Sensitivity* = TP/(TP+FN), *False Alarm* = FP/(FP+TN), *Specificity* = TN/(TN+FP), *Precision* = TP/(TP+FP)

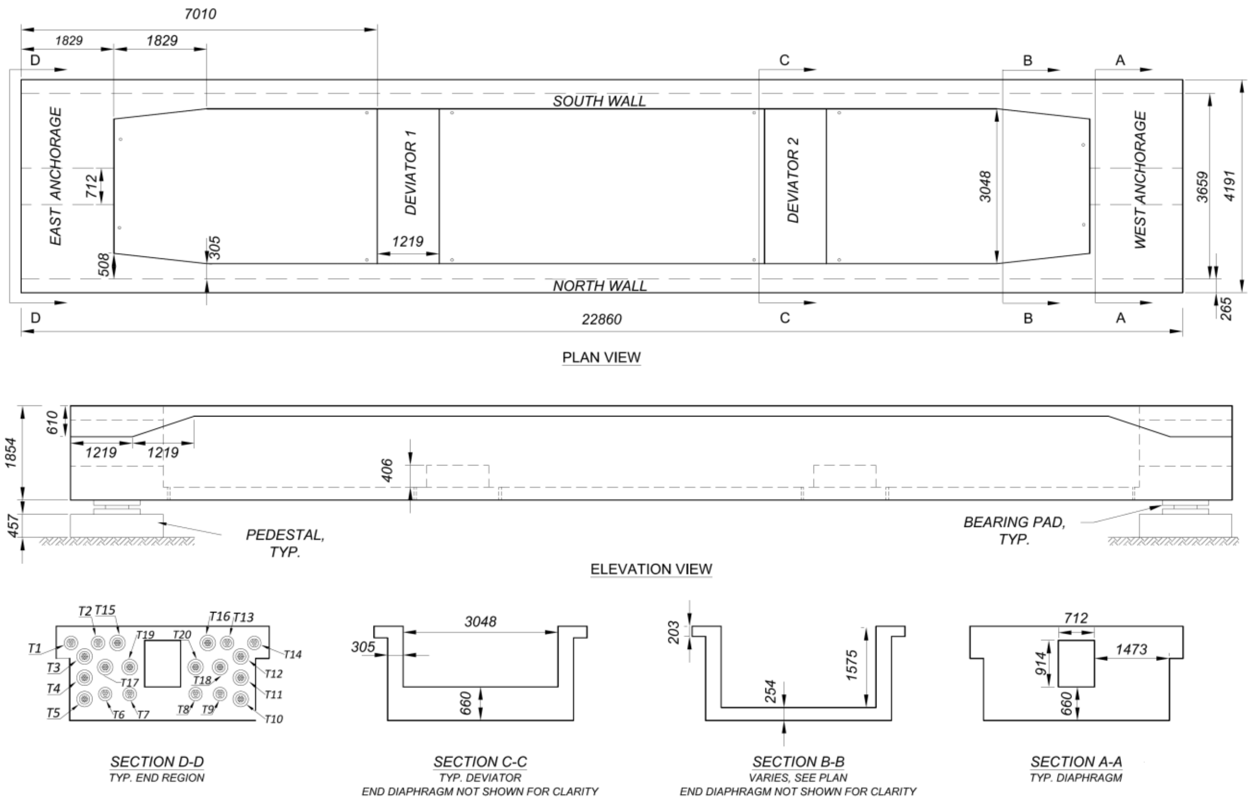

Note: Dimensions are in millimeters.

Fig. 1–Layout and cross-sectional details of post-tensioned U-girder specimen.

(a) Corrugated plastic ducts within the web and flange of the South Wall

(b) Metal ducts within the web and flange of the North Wall

(c) Draped internal tendons

(d) Finished PT U-girder specimen

Fig. 2–PT U-girder construction with draped internal tendons.

(a) StructureScan Mini HR GPR unit

(b) IE scanner and DAQ PC

(c) UST inspection using A1040 MIRA ultrasonic tomograph

(e) Transducer layout of A1040 MIRA

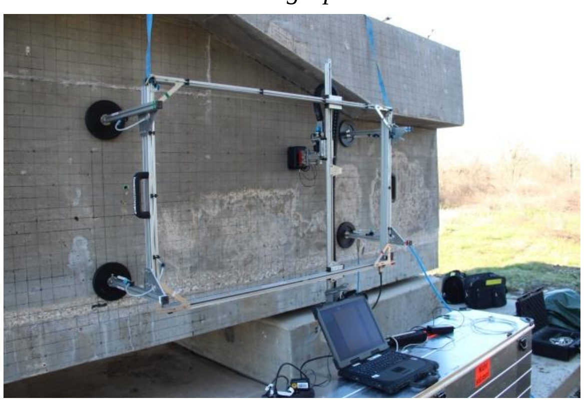

(d) USE inspection with dual element probe mounted on an automated scanner

(f) Point contact transducer probe

Fig. 3–NDE equipment used for the inspection of internal tendons.

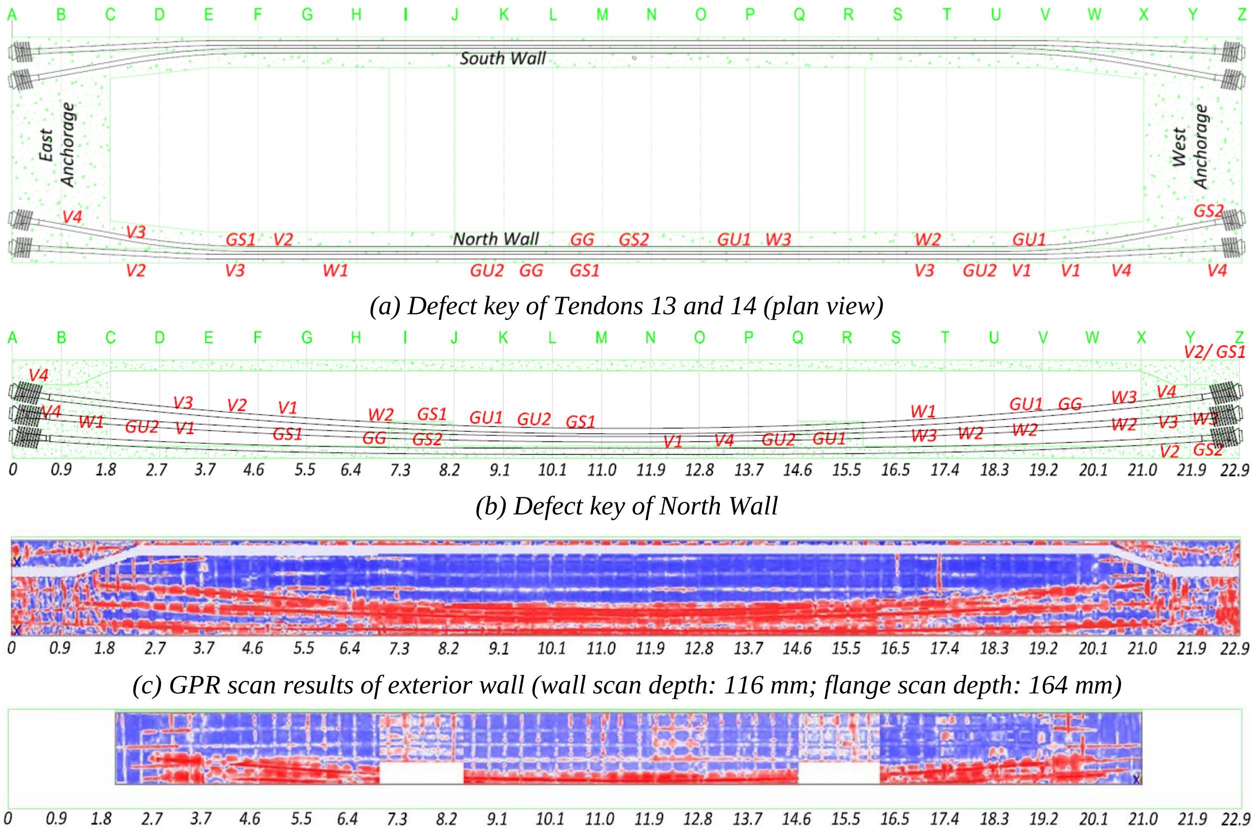

(a) Defect key of Tendons 13 and 14 (plan view)

(b) Defect key of North Wall

(c) GPR scan results of exterior wall (wall scan depth: 116 mm; flange scan depth: 164 mm)

(d) GPR scan results of interior wall (wall scan depth: 137 mm)

Fig. 4– Comparison of GPR scan results from the North Wall of the PT girder specimen with the defect key.

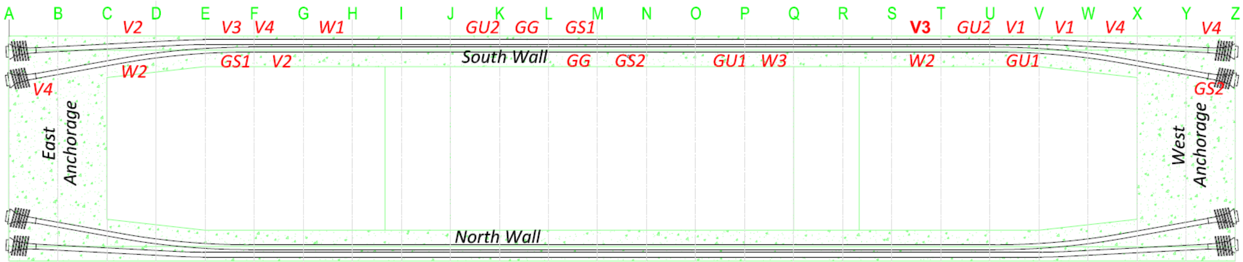

(a) Defect key of Tendons 1 and 2 (plan view)

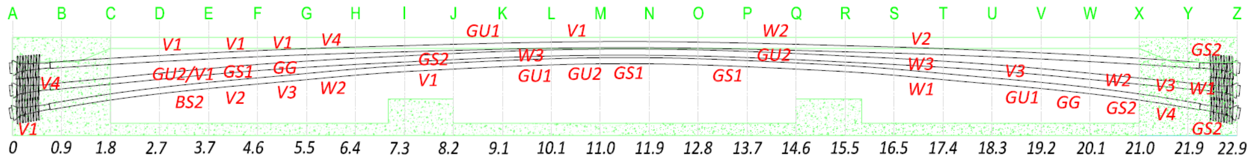

(b) Defect key of South Wall

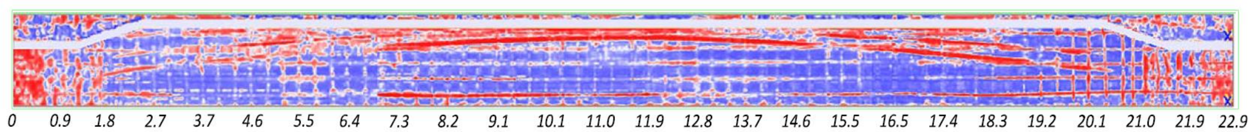

(c) GPR scan results of exterior wall (wall scan depth: 121 mm; flange scan depth: 154 mm.)

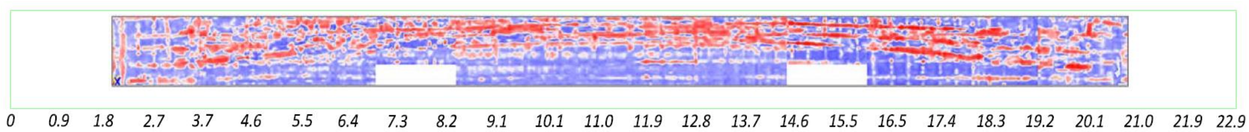

(d) GPR scan results of interior wall (wall scan depth: 136 mm)

Fig. 5–Comparison of GPR scan results from the South Wall of the PT girder specimen with the defect key.

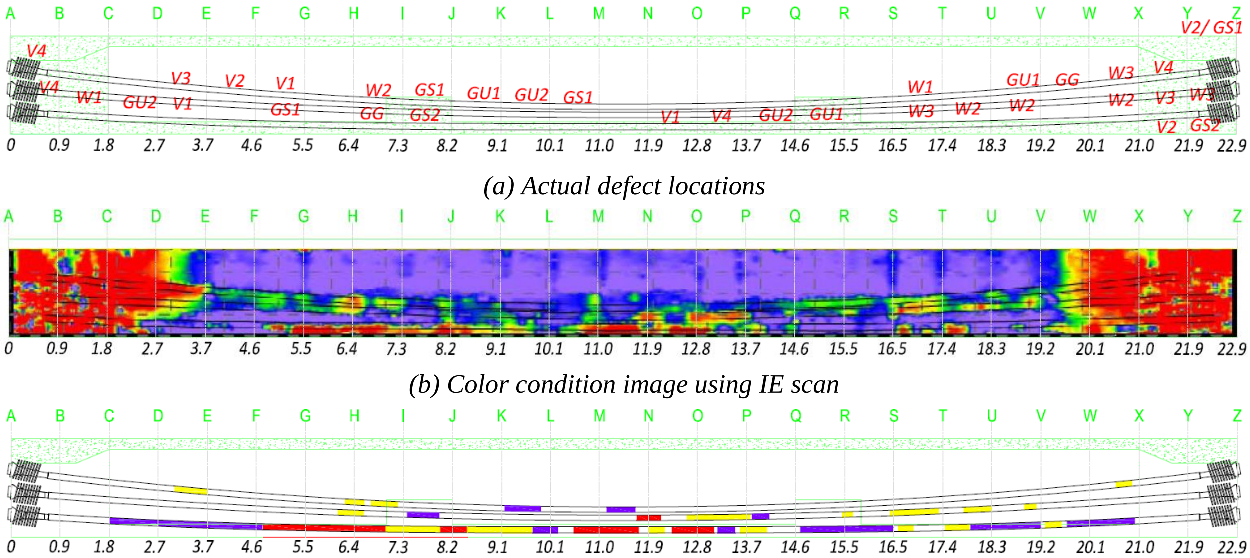

(a) Actual defect locations

(b) Color condition image using IE scan

(c) Defect condition identified using IE testing

Note: Red = Full void, Yellow = Partial void, Purple = Tendon is not detected. Blue-Green in (b) shows intact regions, which are left white in (c).

Fig. 6–Comparison of results from IE with defect key – North Wall web of PT girder specimen.

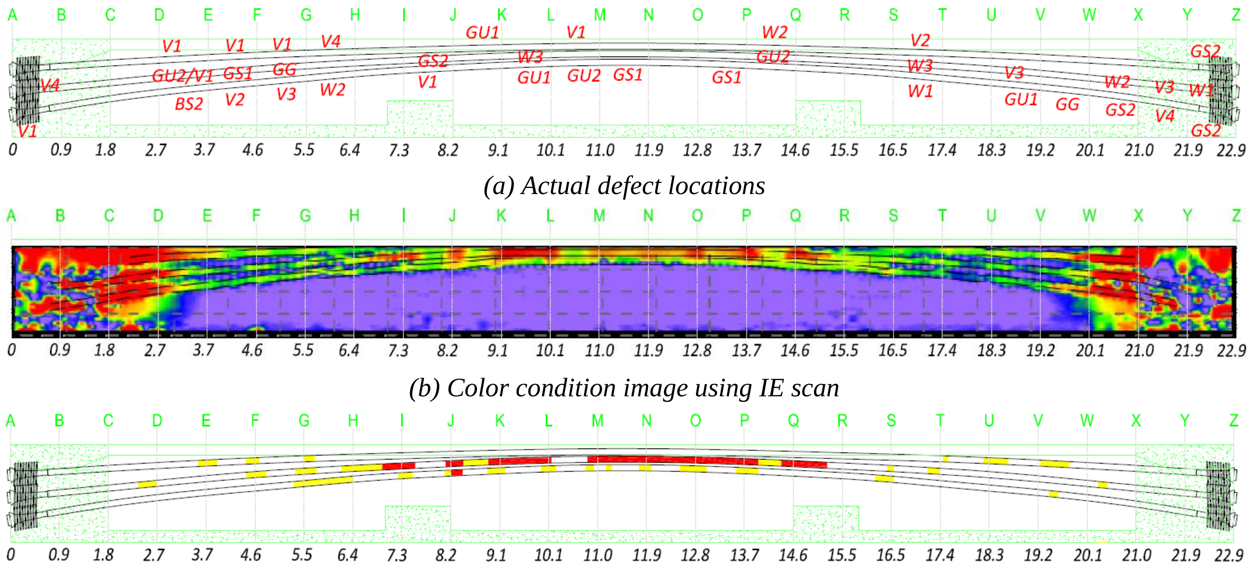

(a) Actual defect locations

(b) Color condition image using IE scan

(c) Defect condition identified using IE testing

Note: Red = Full void, Yellow = Partial void, Purple = Tendon is not detected. Blue-Green in (b) shows intact regions, which is not shown in (c).

Fig. 7–Comparison of results from IE with defect key – South Wall web of PT girder specimen.

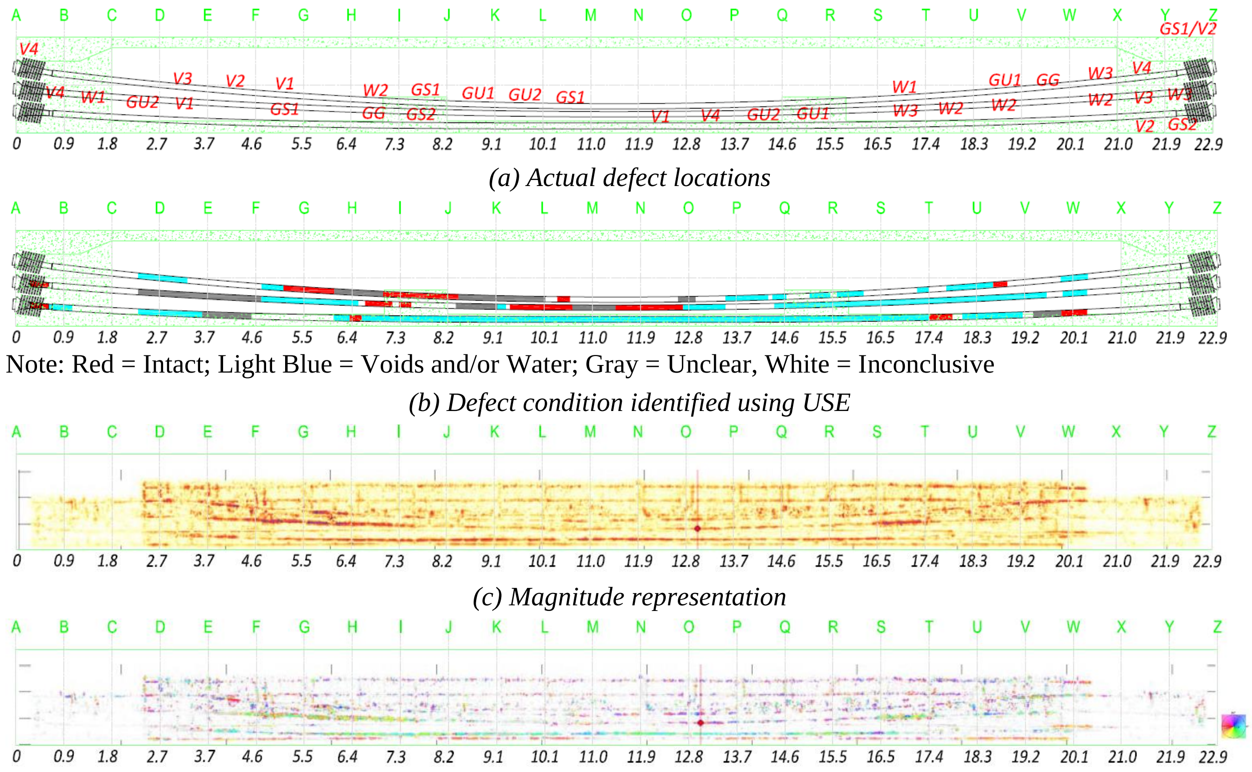

(a) Actual defect locations

Note: Red = Intact; Light Blue = Voids and/or Water; Gray = Unclear, White = Inconclusive

(b) Defect condition identified using USE

(c) Magnitude representation

(d) Phase representation

Fig. 8–Comparison of USE scan results with defect key – exterior North Wall of PT girder specimen.

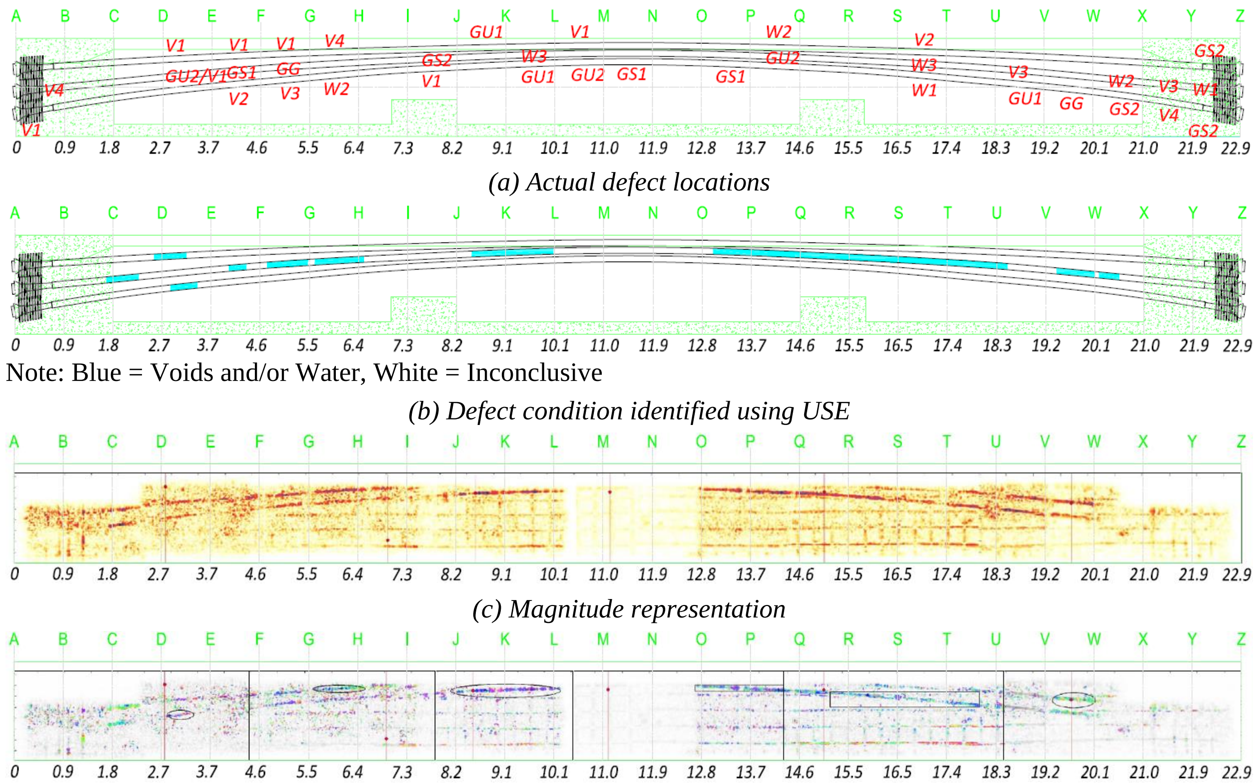

(a) Actual defect locations

(b) Defect condition identified using USE

(c) Magnitude representation

(d) Phase representation

Fig. 9–Comparison of USE results with defect key – exterior South Wall of PT girder specimen.

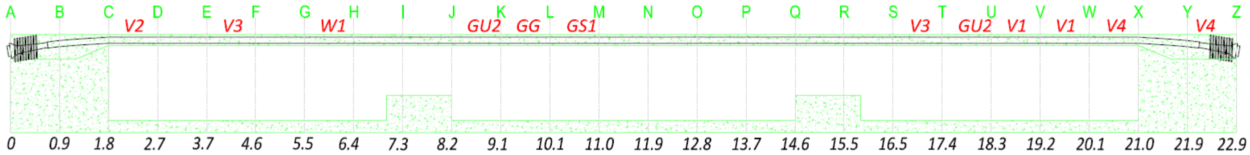

(a) Defect key of Tendon 14

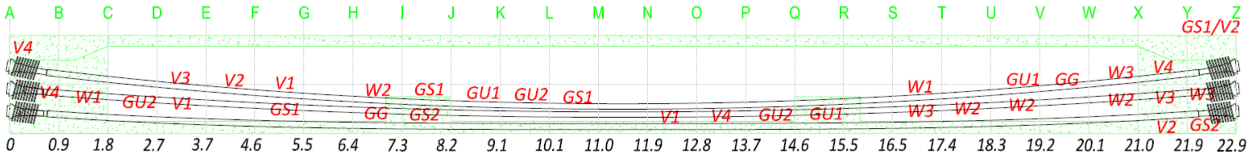

(b) Defect key of North Wall

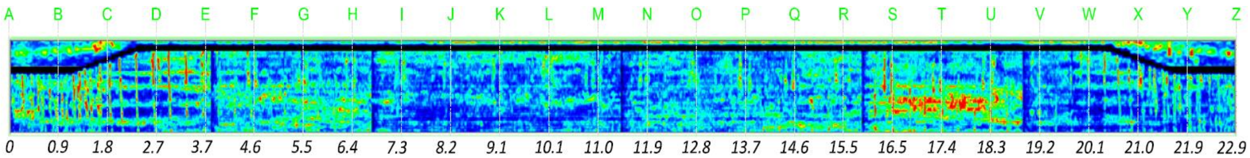

(c) MIRA scan – parallel to tendons (wall scan depth: 73 – 245 mm; flange scan depth: 165 – 245 mm)

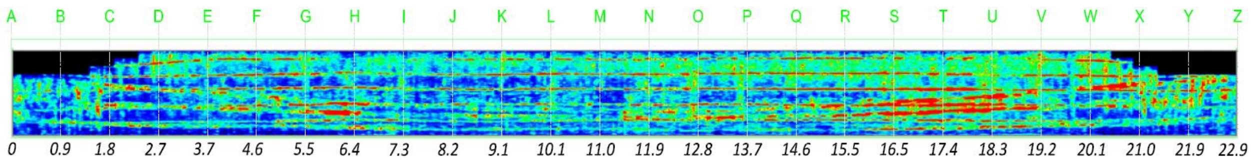

(d) MIRA scan – perpendicular to tendons (wall scan depth:73 – 245 mm)

Fig. 10–Comparison of UST scan results from the North Wall of the PT girder specimen with the defect key.

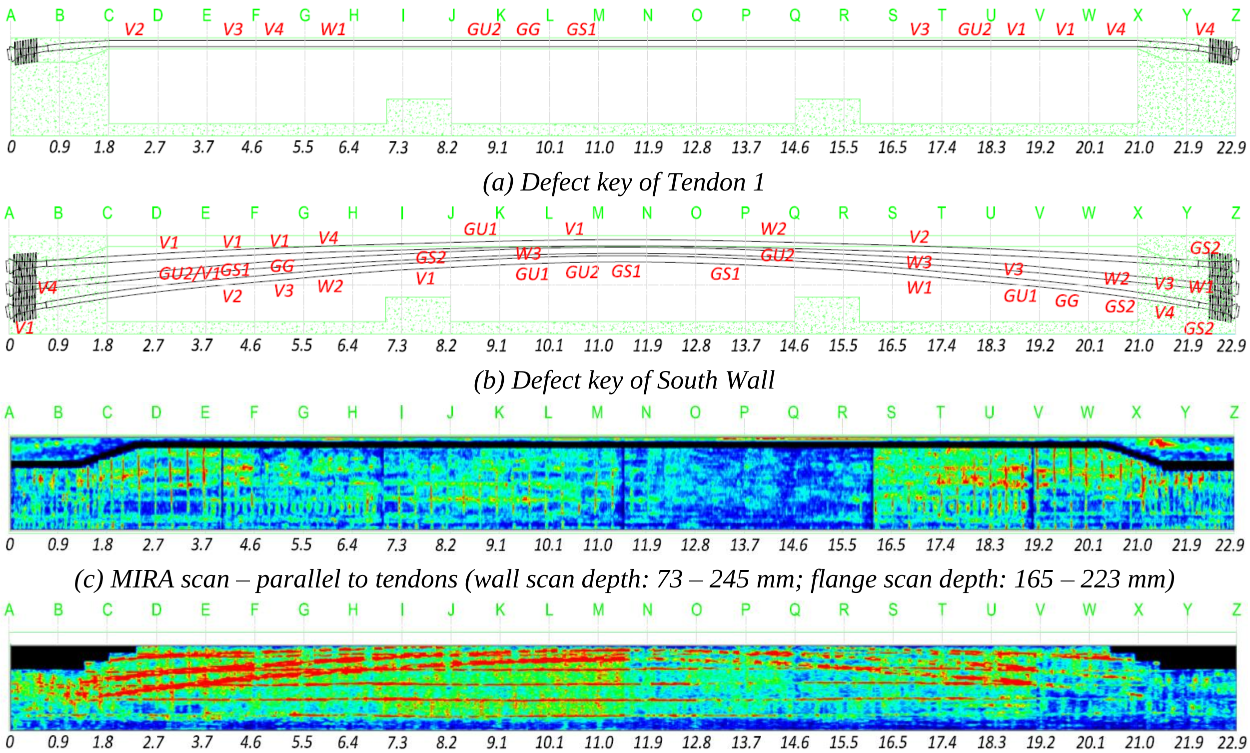

(a) Defect key of Tendon 1

(b) Defect key of South Wall

(c) MIRA scan – parallel to tendons (wall scan depth: 73 – 245 mm; flange scan depth: 165 – 223 mm)

(d) MIRA scan – perpendicular to tendons (wall scan depth:73 – 245 mm)

Fig. 11–Comparison of UST scan results from exterior South Wall of the PT girder specimen with the defect key.

REFERENCES

[1] Martin J., Broughton K. J., Giannopolous A., Hardy M. S. A., Forde M. C. Ultrasonic Tomography of Grouted Duct Post-Tensioned Reinforced Concrete Bridge Beams. NDT & E International. 2001;34:107-13.

[2] Poston R. W., Wouters J. P. Durability of Precast Segmental Bridges. NCHRP Web Document No. 15. National Cooperative Highway Research Council, Transportation Research Board, National Research Council, Washington, DC; 1998.

[3] Corven Engineering Inc. New Directions for Florida Post-Tensioned Bridges. Florida Department of Transportation, Tallahassee, Florida; 2002.

[4] Shahawy M., Cox W. R. Critical Evaluation and Condition Assessment of Posttensioned Bridges in Texas. 6th International Bridge Engineering Conference: Reliability, Security, and Sustainability in Bridge Engineering. Boston, MA; 2005, p. 257-64.

[5] Bungey J. H., Millard S. G., Shaw M. R. Radar Assessment of Post-Tensioned Concrete. Proceeding, 7th International Conference on Structural Faults and Repair. Edinburgh, UK; 1997, p. 331-9.

[6] Wimsatt A., Scullion T., Ragsdale J., Servos S. The Use of Ground Penetrating Radar Data in Pavement Rehabilitation Strategy Selection and Pavement Condition Assessment. Structural Materials Technology III, Bellingham: Proceedings of SPIE. 1998, p. 372-83.

[7] Chung T., Carter C., Masliwec T., Manning D. Impulse Radar Evaluation of Asphalt-Covered Bridge Decks. Aerospace and Electronic Systems, IEEE Transactions on. 1992;28:125-37.

[8] Kohl C., Krause M., Maierhofer C., Wöstmann J. 2D-and 3D-Visualisation of NDT-Data Using Data Fusion Technique. Materials and structures. 2005;38:817-26.

[9] Minchin R. E., Baciak J., Haghighat A. Identification and Demonstration of a Technology Adaptable to Locating Water in Post-Tensioned Bridge Tendons. Transportation Research Board 87th Annual Meeting. Washington, DC; 2006.

[10] Muldoon R., Chalker A., Forde M., Ohtsu M., Kunisue F. Identifying Voids in Plastic Ducts in Post-Tensioning Prestressed Concrete Members by Resonant Frequency of Impact–Echo, SIBIE and Tomography. Construction and Building Materials. 2007;21:527-37.

[11] Pollock D. G., Dupuis K. J., Lacour B., Olsen K. R. Detection of voids in prestressed concrete bridges using thermal imaging and ground-penetrating radar. Report WA-RD 717.1. Washington State Department of Transportation, Transportation Research Board, Olympia, WA; 2008.

[12] Maierhofer C., Krause M., Mielentz F., Streicher D., Milmann B., Gardei A., Kohl C., Wiggenhauser H. Complementary Application of Radar, Impact-Echo, and Ultrasonics for Testing Concrete Structures and Metallic Tendon Ducts. Transportation Research Record: Journal of the Transportation Research Board. 2004;1892:170-7.

[13] Cruz P. J., Topczewski L., Fernandes F. M., Trela C., Lourenço P. B. Application of Radar Techniques to the Verification of Design Plans and the Detection of Defects in Concrete Bridges. Structure and Infrastructure Engineering. 2010;6:395-407.

[14] Derobert X., Aubagnac C., Abraham O. Comparison of NDT Techniques on a Post-Tensioned Beam Before its Autopsy. NDT & E International. 2002;35:541-8.

[15] Wimsatt A., White J., Leung C., Scullion T., Hurlebaus S., Zollinger D., Grasley Z., Nazarian S., Azari H., Yuan D., Shokouhi P., Saarenketo T. Mapping Voids, Debonding, Delaminations, Moisture, and Other Defects Behind or Within Tunnel Linings. Strategic Highway Research Program 2, Washington, D.C.; 2014.

[16] Sansalone M., Carino N. J. Laboratory and Field Studies of the Impact-Echo Method for Flaw Detection in Concrete. ACI Special Publication. 1989;112:1-20.

[17] Carino N. J., Sansalone M. Detection of Voids in Grouted Ducts Using the Impact-Echo Method. ACI Materials Journal. 1992;89:296-303.

[18] Shokouhi P., Gucunski N., Wiggenhauser H. Using Impact Echo for Nondestructive Detection of Delaminations in Concrete Bridge Decks. Proceedings of the 6th International Symposium on NDT in Civil Engineering. St. Louis, MO; 2006.

[19] Celaya M., Shokouhi P., Nazarian S. Assessment of Debonding in Concrete Slabs using Seismic Methods. Transportation Research Record: Journal of Transportation Research Board. 2007;2016:65-75.

[20] Shokouhi P., Gucunski N. Application of Impact Echo in Long Term Condition Monitoring of Concrete Bridge Decks – A Numerical Study. ASCE Geotechnical Special Publication (GPS). 2007;164:1-12.

[21] Shokouhi P. Two-Channel Impact Echo. NDTCE’09, Non-Destructive Testing in Civil Engineering. Nantes, France; 2009, p. 8.

[22] Breysse D. Non-Destructive Assessment of Concrete Structures: Reliability and Limits of Single and Combined Techniques. Dordrecht, NLD: Springer; 2012.

[23] Tinkey Y., Olson L. Applications and limitations of impact echo scanning for void detection in posttensioned bridge ducts. Transportation Research Record: Journal of the Transportation Research Board. 2008:8-12.

[24] Tinkey Y., Olson L., Wiggenhauser H. Impact Echo Scanning for Discontinuity Detection and Imaging in Posttensioned Concrete Bridges and Other Structures. Materials evaluation. 2005;63:64-9.

[25] Harris D. M. J. M. Test and Assessment of NDT Methods for Post Tensioning Systems in Segmental Balanced Cantilever Concrete Bridges. Central Structures Office, Florida Department of Transportation, Tallahassee, Florida; 2003.

[26] Zhu J., Popovics J. S. Imaging Concrete Structures Using Air-Coupled Impact-Echo. Journal of Engineering Mechanics. 2007;133:628-40.

[27] Ata N., Mihara S., Ohtsu M. Imaging of ungrouted tendon ducts in prestressed concrete by improved SIBIE. NDT & E International. 2007;40:258-64.

[28] Ohtsu M., Yamada M., Nakai Y. Identification of Ungrouted Tendon Duct in Prestressed Concrete by SIBIE. Non-Destructive Testing in Civil Engineering. Nantes, France; 2009.

[29] Krause M., Maierhofer C., Wiggenhauser H. Thickness Measurement of Concrete Elements using Radar and Ultrasonic Impulse Echo Techniques. Proc 6th International Conf on Structural Faults and Repair. London, UK; 1995, p. 17-24.

[30] Krause M., Bärmann M., Frielinghaus R., Kretzschmar F., Kroggel O., Langenberg K., Maierhofer C., Müller W., Neisecke J., Schickert M. Comparison of pulse-echo methods for testing concrete. NDT & E International. 1997;30:195-204.

[31] Schickert M. Towards SAFT-Imaging in Ultrasonic Inspection of Concrete. International Symposium Non Destructive Testing in Civil Engineering (NDT-CE). 1995, p. 411-148.

[32] Schickert M., Krause M., Müller W. Ultrasonic Imaging of Concrete Elements Using Reconstruction by Synthetic Aperture Focusing Technique. Journal of Materials in Civil Engineering. 2003;15:235-46.

[33] Iyer S., Schokker A. J., Sinha S. K. Ultrasonic C-scan imaging: Preliminary evaluation for corrosion and void detection in posttensioned tendons. Transportation Research Record: Journal of the Transportation Research Board. 2003;1827:44-52.

[34] Im S. B., Hurlebaus S. Non-Destructive Testing Methods to Identify Voids in External Post-Tensioned Tendons. KSCE Journal of Civil Engineering. 2012;16:388-97.

[35] Im S. B., Hurlebaus S., Trejo D. Inspection of Voids in External Post-tensioned Tendons. Transportation Research Record: Journal of the Transportation Research Board. 2010;2172:115-22.

[36] Mayer K., Langenberg K.-J., Krause M., Milmann B., Mielentz F. Characterization of reflector types by phase-sensitive ultrasonic data processing and imaging. Journal of Nondestructive Evaluation. 2008;27:35-45.

[37] Krause M., Mayer K., Friese M., Milmann B., Mielentz F., Ballier G. Progress in Ultrasonic Tendon Duct Imaging. European Journal of Environmental and Civil Engineering. 2011;15:461-85.

[38] Hurlebaus S., Hueste M. B. D., Karthik M. M., Terzioglu T. Inspection Guidelines for Bridge Post-Tensioning and Stay Cable Systems Using NDE Methods. NCHRP Report 14-28. National Cooperative Highway Research Program, Transportation Research Board of The National Academies, Washington, DC; 2017.

[39] Hurlebaus S., Hueste M. B. D., Karthik M. M., Terzioglu T. Condition Assessment of Bridge Post-tensioning and Stay Cable Systems Using NDE Methods. NCHRP Report 14-28. National Cooperative Highway Research Program, Transportation Research Board of The National Academies, Washington, DC; 2017.